Enhanced Proton Acceleration by an Ultrashort Laser Interaction with Structured Dynamic Plasma Targets

A. Zigler,[1] S. Eisenman,[1] M. Botton,[1,*] E. Nahum,[1] E. Schleifer,[1] A. Baspaly,[1] I. Pomerantz,[1] F. Abicht,[2] J. Branzel,[2] G. Priebe,[2] S. Steinke,[2] A. Andreev,[2] M. Schnuerer,[2] W. Sandner,[2] D. Gordon,[3] P. Sprangle,[3] and K. W. D. Ledingham[4]

[1]*Racah Institute of Physics, The Hebrew University of Jerusalem, Jerusalem 91904, Israel*
[2]*Max Born Institute, Berlin D-12489, Germany*
[3]*Plasma Physics Division, Naval Research Laboratory, Washington, DC 20375, USA*
[4]*University of Strathclyde, Glasgow G4 0NG, Scotland, United Kingdom*

(Received 31 January 2013; published 21 May 2013)

We experimentally demonstrate a notably enhanced acceleration of protons to high energy by relatively modest ultrashort laser pulses and structured dynamical plasma targets. Realized by special deposition of snow targets on sapphire substrates and using carefully planned prepulses, high proton yields emitted in a narrow solid angle with energy above 21 MeV were detected from a 5 TW laser. Our simulations predict that using the proposed scheme protons can be accelerated to energies above 150 MeV by 100 TW laser systems.

DOI: 10.1103/PhysRevLett.110.215004 PACS numbers: 52.38.Kd, 41.75.Jv, 52.35.Mw, 52.65.Rr

Proton acceleration by the interaction of an ultra high intensity laser beam with matter has several wide prospective applications including cancer treatment, astrophysics in the lab, nuclear physics, and material sciences (see Refs. [1,2] for a review). Over the years several promising acceleration schemes were proposed and demonstrated, such as target normal sheath acceleration (TNSA) [3–5], radiation pressure acceleration [6,7], break-out afterburner acceleration [8], and collisionless shock acceleration [9]. Variations of these schemes including mass-limited targets [10] and nanostructure targets [11–13] aimed at increasing the efficiency of the interaction were also considered. Some of these schemes require an exceedingly high intensity of the laser beam in order to initiate the process, and most of them require a laser energy exceeding a 1 PW level (on target) in order to accelerate the protons to energies of about 150 MeV required by medical applications. Furthermore, all of these schemes pose the same requirement that the laser system have an energy as low as possible stored in the prepulse. The main reason is that these accelerating schemes are optimized for an interaction between the main pulse and a cold solid-density target, and are strongly degraded as the main laser pulse interacts with a preheated (or even ionized) target. It was recently shown that preformed plasma may be beneficial to the acceleration process [14,15]. Nevertheless, the majority of the experiments still aim at cold targets with a prepulse as low as possible. Accordingly, achieving such a low energy content in the prepulse requires a contrast ratio of the order of 10^{-11} for a 100 TW laser and even higher for more energetic systems, which is a real experimental challenge.

In this Letter we report for the first time on the acceleration of proton bunches to energies above 21 MeV by a 5 TW ultrashort (50 fs) laser pulse. We introduce an alternative approach to the laser-based proton acceleration quest by using a moderate power (<10 TW) laser system, and carefully produced microstructured snow targets [16,17]. Our experimental results show that the energy of the accelerated protons scales with the power of the laser according to the $E_p \propto {P_L}^{1/2}$ rule which is obtained here for significantly lower laser powers than for traditional schemes. Numerical 2D PIC code simulations of the interaction process reproduce the experimentally obtained scaling law and predict the possibility of accelerating protons to 150 MeV with a laser power of about 100 TW. This notably increased proton energy is attributed to a combination of three mechanisms. First is the localized enhancement of the laser field intensity near the tip of the microstructured whisker. This causes an increased electronic charge repulsion out of the whisker. Second is a mass-limited-like phenomena, namely the absence of a high density cold electron cloud in the vicinity of the whisker which can compensate for the expelled electrons. The heated electrons remain in the vicinity of the positively charged whisker, producing strong accelerating electrostatic fields and pulling the protons out. Third is the Coulomb explosion of the positively charged whisker, adding a longtime acceleration to the protons. As our innovative microstructured snow scheme requires the interaction of the laser with a structured dynamical plasma target, it also relaxes the requirements of a high contrast ratio for the laser system, and facilitates the production of the target.

Two separate laser systems were used to obtain the results reported here. One is the laser at the High-Intensity Laser Lab at the Hebrew University of Jerusalem (HUJI) and the other is the laser system at the Max Born Institute at Berlin (MBI). The HUJI system is a 2 TW, 50 fs pulse length laser operating at a central wavelength of 0.8 μ. The spot size (FWHM) is as small as 20 μm^2. The contrast ratio of the HUJI system is about

1000, dictated by the leakage of the regenerative amplifier; thus, the prepulse is shaped similarly to the main pulse and arrives on the target approximately 10 nsec before the main pulse. The MBI system is a 30 TW, 70 fs 0.8 μ laser. The beam is focused to a spot size of 5 μ on target. The contrast ratio of the MBI system is about 10^{-8}, and the prepulse is a pedestal-like shape. In order to obtain the same preplasma conditions in both institutes, the main beam at the MBI system is split and a prepulse is artificially formed. The experiments at the MBI site were carried out using a 0.03 mJ prepulse, 6 ns ahead of the main pulse.

A schematic diagram of the experimental setup in both institutes is shown in Fig. 1. The laser beam strikes the target at a 60° angle to the normal. The target is a liquid nitrogen cooled sapphire substrate on which water vapor is deposited. The size and density of the snow pillars as well as the surface roughness are determined by various parameters such as pressure, flow, and temperature.

Figure 2 shows typical snow targets as imaged by a scanning electron microscope. The snow surface can be characterized as a highly structured surface with essentially three roughness scales: (a) pillars of about 100 μ, (b) spikes of about 10 μ on top of them, and (c) whiskers of about 1 μ on the spikes. The distribution of the pillars and spikes is controlled by seeding and fixing the flow of the vapor. The red circle in Fig. 2 schematically represents the laser spot (prepulse and main pulse) for a typical shot. Based on our measurements of the laser spot characteristics, we estimate that the laser spot interacts with few (typically less than 5) whiskers. The prepulse meets the whiskers. Theoretical estimates show that due to its low energy content ($\lesssim 0.05$ mJ) the prepulse can vaporize only the thin external layer of the few illuminated whiskers. The target therefore keeps its shape but is locally surrounded by a highly nonuniform plasma. The time delay between the prepulse and main pulse is about 10 ns, during which the plasma can freely expand and a highly nonuniform plasma cloud is formed. By the time of its arrival, the main pulse meets this highly structured dynamic plasma cloud and interacts with it to produce the accelerated protons.

The main diagnostics consists of stacks of CR39 film, each of 25 mm diameter. The thickness of the CR39 is 1.5 mm. In front of the first CR39 film we positioned a 13 μ aluminum foil which prevents the plasma plume emitted in the process from damaging the films. The detector films are positioned at a distance of about 2.5 cm from the target at an angle of 45°. The setup enables sufficient energy and spatial resolution. The CR39 plates are replaced every several laser shots (typically 3–5) and the exposed films are etched using the conventional methods. Analysis of the processed CR39 consisted of automated counting of the pits and comparing the resulting number to unexposed areas on the same film and on a reference (processed) film. Exposed areas in all the films showed a clear signal far above the noise level, which is unquestionably the result of accelerated protons. Figure 3 shows a 100×100 μ area of three processed CR39 films. The first plate was uniformly covered by proton tracks. Considering the thickness of the foil that covered the stack it is concluded that the tracks are produced by protons of energy above 1 MeV. The second CR39 detector was covered by a lower density but still uniform distribution of tracks. These are attributed to protons of energy above 13 MeV. The tracks marked on the third plate are the result of protons with energy above 20 MeV. Here the density is not uniform and bunches can be seen.

We have repeated the experiment with various laser power levels to produce the energy scaling of the most energetic protons accelerated of the snow targets (see Fig. 4). The fitted scaling from this data set of this novel acceleration scheme is $E_p \propto P_L^{0.58}$, and is obtained with lower laser power levels. Notice that unlike the traditional TNSA scheme there is no clear distinction of the back and front surface as the laser does not cross the target but interacts with its microstructured surface and the plasma cloud generated there by the prepulse. At this point we note that when the prepulse was not present and the main pulse interacted directly with the snow surface, the resulting protons were accelerated to a much lower energy level,

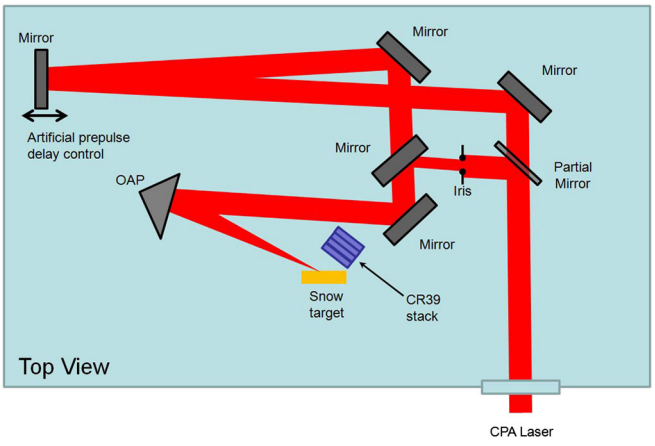

FIG. 1 (color online). The experimental setup.

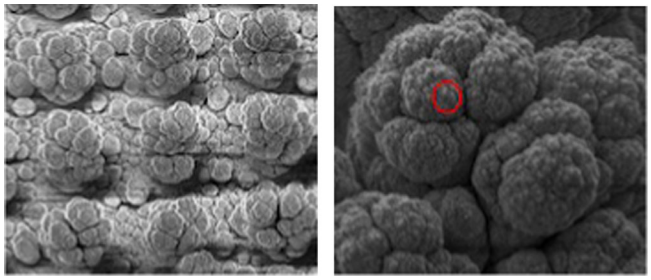

FIG. 2 (color online). Scanning electron microscope images of the snow targets. Total width shown is 1000 μ (a) and 100 μ (b). Red circle represents the laser spot.

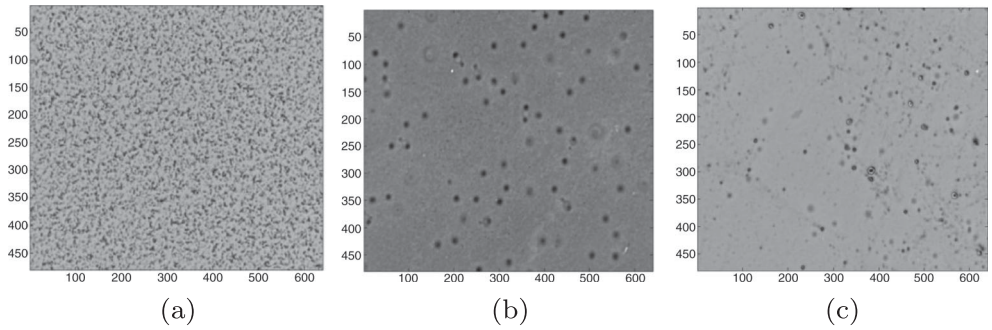

FIG. 3. Processed CR39 showing marks of protons with (a) energy >1 MeV, (b) energy >13 MeV, (c) energy >20 MeV.

down to the traditional scaling of the TNSA scheme. A count of the total number of tracks on the CR39 detector plates is shown in the inset of Fig. 4. The measured energy spectrum is not a monotonically decreasing function of the energy (within the available resolution) and a clear peak is evident at energies around 20 MeV. We also found that the most energetic protons were found on the CR39 detectors at a location which is close to the position of a reflected laser field for a planar target. The total count of high energy protons (above 20 MeV) is 10^6 protons per shot, and above 10^8 over all energy protons per shot. The estimated efficiency of laser energy conversion to proton energy is about 10^{-3}. The laser interacts with the small scale whisker at the edge of larger scale structures, the tips and the pillars. The interaction therefore strongly depends on the exact position of the laser spot on the highly structured surface. This leads to shot to shot fluctuations in the maximum energy of the protons as well as the total flux. We are currently developing an *in situ* visual aiming system that will enable micron scale positioning of the laser spot on the target and hence reduce the shot to shot fluctuations.

The TURBOWAVE particle in cell (PIC) [18] simulations of the acceleration scheme presented here are based on the one dimensional model presented in our previous work [17] which demonstrated the significant enhancement by the local plasma density near the whisker tip. Considering the size scales of the target and the laser spot size we focus our study on the interaction of the laser with a single snow whisker. Following the prepulse illumination, the whisker is partially vaporized and ionized; hence, a nonuniform plasma cloud (protons, triply ionized oxygen, and electrons) is formed. We model this highly structured dynamic plasma as an ellipsoid. We estimate that the high ($\sim 100 n_{cr}$, where $n_{cr} = 1.1 \times 10^{21}/\lambda^2$ is the traditional critical density) density portion of the whisker is an ellipsoid of the order of 0.1–0.2 μ width (minor axis) and 1–2 μ length (major axis). Estimates of the density gradients of the plasma cloud (supported by the 1D hydrocode HYADES [19]) set the critical density contour to be an ellipsoid of the order of 1–2 μ width (minor axis) and 10 μ length (major axis). The linearly polarized laser has a spot size of 5 μ and is taken to hit the plasma cloud at an angle of 45° with respect to the major axis. A schematic of the plasma cloud and the laser pulse is shown in Fig. 5(a). The laser pulse is of 88 fs total duration with a linear rise time and fall time of 32 fs each. Further simplification is achieved by eliminating one dimension and setting the whisker to be independent of the y coordinate (hence it becomes a wedge), keeping the polarization of the laser in the x-z plane. The 2D model is expected to reproduce the energy scaling of the accelerated protons but not the spatial

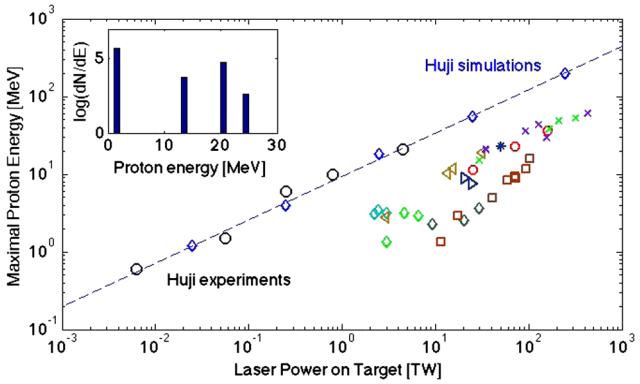

FIG. 4 (color online). Energy scaling of the accelerated protons as a function of the laser power on target. Various points describe data obtained by many contributors [20–37]. (See Ref. [38] for details.)

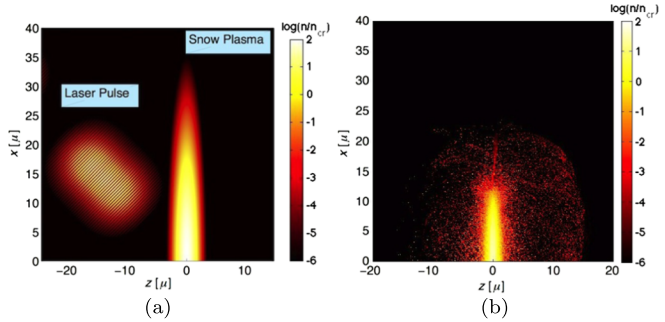

FIG. 5 (color online). (a) Schematic drawing of the simulation setup. The plasma density is normalized to the critical density shown in the logarithmic color map. The laser intensity is not to scale. (b) The electron density at 88 fs.

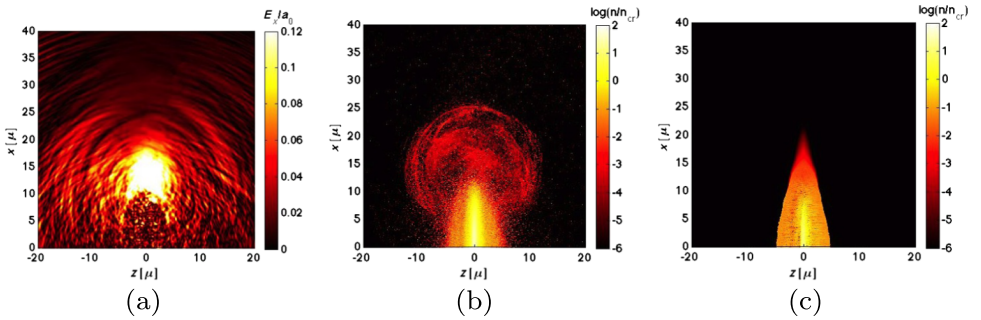

FIG. 6 (color online). (a) The intensity of the x component of the electric field, in normalized units ($a_0 = eE/mc\omega$), at 220 fs. Electron density (b) and proton density (c) normalized to critical density at 220 fs.

distribution which will be strongly dependent on the angle between the polarized field and the major axis of the plasma ellipsoid as well as other neighboring whiskers which affect the propagation of the laser field. The cell size is $0.05 \times 0.05\ \mu$, and the simulation region is $200 \times 200\ \mu$.

The interaction and acceleration process is roughly separated into three phases. In the first phase, which is approximately the laser pulse duration, the laser drives the electrons out of the plasma ellipsoid. These electrons are accelerated by the laser's ponderomotive potential and part of them escapes out of the plasma cloud leaving the heavy highly charged oxygen atoms and the protons behind [see Fig. 5(b)]. The curved equal density surfaces affect the ponderomotive potential force. Unlike the TNSA target, there is no clear distinction between back and front surfaces as they are mixed over the whisker tip. Plotting the density of the electrons at 88 fs (one pulse length) as shown in Fig. 5(b) demonstrates these properties. A runaway electron stream can be seen along $z = 0$ and $x \geq 15\ \mu$. Just below them ($10\ \mu \geq x \leq 15\ \mu$) electrons start to accumulate near the tip of the whisker. The second phase is a short time after the passage of the laser pulse, approximately a 2–3 pulse duration. The second acceleration phase is described in Fig. 6. The axial component of the electric field shows intense enhancement near the tip [white spot at the center of Fig 6(a)] which is the result of the electron accumulation [red spherical cloud at the center of Fig. 6(b)]. The ions [see Fig. 6(c)] at that time are accelerated by the localized fields. The third and last phase is the extended time acceleration, around a 3–6 laser pulse duration. The accelerating field is maintained by the charge separation and can be seen as the bright bow in Fig. 7(a). The electron accumulation near the whisker tip is reduced but charge separation between the electrons and ions is maintained [see Fig. 7(b)]. The protons [see Fig. 7(c)] are accelerated by the field and are pushed by the heavier oxygen ions. The highest energy of the protons for this simulation was found to be 15 MeV. The scaling law of Fig. 4 was obtained by repeating the simulations with changed laser power.

In conclusion, we have experimentally demonstrated the acceleration of protons to energy up to 21 MeV by a modest power (~ 5 TW) laser. The acceleration scheme is based on a highly structured dynamic plasma target which is produced by a prepulse illumination of a snow target. The energy scaling resembles the power law of planar targets but is obtained with a much lower laser energy. The proton yield is of the order of 10^6 protons per shot with an angular distribution of the high energy component of protons of ~ 0.1 rad. PIC simulations reproduce the energy scaling and predict that by using a 100 TW laser, protons can be accelerated to the 150 MeV level. This is a considerable improvement over alternative

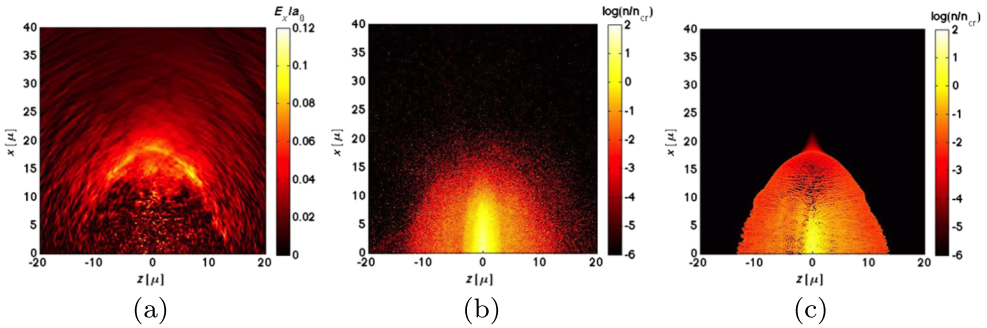

FIG. 7 (color online). (a) The intensity of the x component of the electric field, in normalized units ($a_0 = eE/mc\omega$), at 440 fs. Electron density (b) and proton density (c) normalized to critical density at 440 fs.

acceleration schemes which require a higher energy laser system with an extremely high contrast ratio. The team intends to carry out further experiments at higher laser intensities to see whether the important medical proton energies of about 100 MeV can be reached.

*Corresponding author.
bdmoti@phys.huji.ac.il

[1] K. W. D. Ledingham and W. Galster, New J. Phys. **12**, 045005 (2010).
[2] H. Daido, M. Nishuichi, and A. S. Pirozhkov, Rep. Prog. Phys. **75**, 056401 (2012).
[3] S. Hatchet *et al.*, Phys. Plasmas **7**, 2076 (2000).
[4] S. C. Wilks, A. B. Langdon, T. E. Cowan, M. Roth, M. Singh, S. Hatchett, M. H. Key, D. Pennington, A. MacKinnon, and R. A. Snavely, Phys. Plasmas **8**, 542 (2001).
[5] S. A. Gaillard *et al.*, in *Proceedings of the APS 51st Annual Meeting of the Division of Plasma Physics*, Vol. 54 (Bulletin of the American Physical Society, New York, 2009), Abstract No. G06.003.
[6] T. Esirkepov, M. Borghesi, S. Bulanov, G. Mourou, and T. Tajima, Phys. Rev. Lett. **92**, 175003 (2004).
[7] B. M. Hegelich, B. J. Albright, J. Cobble, K. Flippo, S. Letzring, M. Paffett, H. Ruhl, J. Schreiber, R. K. Schulze, and J. C. Fernández, Nature (London) **439**, 441 (2006).
[8] A. Henig *et al.*, Phys. Rev. Lett. **103**, 045002 (2009).
[9] D. Haberberger, S. Tochitsky, F. Fiuza, C. Gong, R. A. Fonseca, L. O. Silva, W. B. Mori, and C. Joshi, Nat. Phys. **8**, 95 (2011).
[10] S. Steinke *et al.*, Laser Part. Beams **28**, 215 (2010).
[11] H. Schwoerer, S. Pfotenhauer, O. Jäckel, K.-U. Amthor, B. Liesfeld, W. Ziegler, R. Sauerbrey, K. W. D. Ledingham, and T. Esirkepov, Nature (London) **439**, 445 (2006).
[12] D. Margarone *et al.*, Phys. Rev. Lett. **109**, 234801 (2012).
[13] A. A. Andreev, N. Kumar, K. Platonov, and A. Pukhov, Phys. Plasmas **18**, 103103 (2011).
[14] A. R. Holdunkar and N. K. Gupta, Phys. Plasmas **15**, 123104 (2008).
[15] T. Plachan, S. Pecker, Z. Henis, S. Eisenmann, and A. Zigler, Appl. Phys. Lett. **90**, 041501 (2007).
[16] T. Palchan, Z. Henis, A. Y. Faenov, A. I. Magunov, S. A. Pikuz, S. V. Gasilov, I. Yu. Skobelev, and A. Zigler, Appl. Phys. Lett. **91**, 251501 (2007).
[17] A. Zigler *et al.*, Phys. Rev. Lett. **106**, 134801 (2011).
[18] D. F. Gordon, W. Mori, and T. M. Antonsen, Jr., IEEE Trans. Plasma Sci. **28**, 1135 (2000); D. F. Gordon, IEEE Trans. Plasma Sci. **35**, 1486 (2007).
[19] J. T. Larson, in *Radiative Properties of Hot Dense Matter*, edited by W. Goldstein, C. Hooper, J. Gauthier, J. Seely, and R. Lee (World Scientific, Singapore, 1991).
[20] D. Neely, P. Foster, A. Robinson, F. Lindau, O. Lundh, A. Persson, C.-G. Wahlstrom, and P. McKenna, Appl. Phys. Lett. **89**, 021502 (2006).
[21] A. S. Pirozhkov *et al.*, Proc. SPIE Int. Soc. Opt. Eng. **7354**, 735414 (2009).
[22] M. Nishiuchi *et al.*, Appl. Phys. Lett. **94**, 061107 (2009).
[23] S. Steinke and T. Sokollik (private communication).
[24] S. Fritzler, V. Malka, G. Grillon, J. P. Rousseau, F. Burgy, E. Lefebvre, E. d'Humieres, P. McKenna, and K. W. D. Ledingham, Appl. Phys. Lett. **83**, 3039 (2003).
[25] T. Ceccotti, A. Lévy, H. Popescu, F. Réau, P. D'Oliveira, P. Monot, J. Geindre, E. Lefebvre, and Ph. Martin, Phys. Rev. Lett. **99**, 185002 (2007).
[26] I. Spencer *et al.*, Phys. Rev. E **67**, 046402 (2003).
[27] O. Jäckel, Ph.D. thesis, FSU Jena, 2009.
[28] M. Kaluza, J. Schreiber, M. Santala, G. Tsakiris, K. Eidmann, J. Meyer-ter-Vehn, and K. Witte, Phys. Rev. Lett. **93**, 045003 (2004).
[29] A. J. Mackinnon, Y. Sentoku, P. Patel, D. Price, S. Hatchett, M. Key, C. Andersen, R. Snavely, and R. Freeman, Phys. Rev. Lett. **88**, 215006 (2002).
[30] R. A. Snavely *et al.*, Phys. Rev. Lett. **85**, 2945 (2000).
[31] M. Zepf *et al.*, Phys. Plasmas **8**, 2323 (2001).
[32] K. A. Flippo, J. Workman, D. C. Gautier, S. Letzring, R. P. Johnson, and T. Shimada, Rev. Sci. Instrum. **79**, 10E534 (2008).
[33] S. Gaillard and K. A. Flippo (private communication).
[34] L. Robson *et al.*, Nat. Phys. **3**, 58 (2006).
[35] M. Roth (private communication).
[36] J. Fuchs *et al.*, Nat. Phys. **2**, 48 (2005).
[37] J. Schreiber *et al.*, Phys. Rev. Lett. **97**, 045005 (2006).
[38] K. Zeil, S. D. Kraft, S. Bock, M. Bussmann, T. E. Cowan, T. Kluge, J. Metzkes, T. Richter, R. Sauerbrey, and U. Schramm, New J. Phys. **12**, 045015 (2010).